HHS Public Access

Author manuscript

Circ Heart Fail. Author manuscript; available in PMC 2024 August 01.

Published in final edited form as:

Circ Heart Fail. 2023 August ; 16(8): e010294. doi:10.1161/CIRCHEARTFAILURE.122.010294.

Inhibition of Pyk2 improves Cx43 intercalated disc localization, infarct size, and cardiac function in rats with heart failure

Li Zheng, Ph.D.[1], **Gaelle Spagnol, Ph.D.**[1], **Devashri R. Gandhi, M.S.**[2], **Kanika Sharma, B.S.**[2], **Vikas Kumar, Ph.D.**[2], **Kaushik P. Patel, Ph.D.**[3], **Paul L. Sorgen, Ph.D.**[1,*]

[1]Department of Biochemistry and Molecular Biology, University of Nebraska Medical Center, Omaha, NE 68198, USA.

[2]Department of Genetics, Cell Biology, and Anatomy, University of Nebraska Medical Center, Omaha, NE 68198, USA.

[3]Department of Cellular and Integrative Physiology, University of Nebraska Medical Center, Omaha, NE 68198, USA.

Abstract

Background: Heart failure causes changes in Cx43 regulation that are associated with arrhythmic heart disease. Pyk2 is activated in cardiomyopathies and phosphorylates Cx43 to decrease intercellular communication. This study was designed to determine if Pyk2 inhibition improves cardiac function in a myocardial infarction (MI) induced heart failure model in rats.

Methods: MI (ligation of left anterior descending artery) rats were treated with the Pyk2 inhibitor PF4618433. Hemodynamic and structural parameters were monitored in Sham (n=5), MI-vehicle (n=5), and MI-PF4618433 (n=8) groups. Heart tissues were collected after 6-weeks to assess Pyk2 and Cx43 protein level and localization.

Results: PF4618433 produced no observed adverse effects and inhibited ventricular Pyk2. PF4618433 reduced the MI infarct size from 34% to 17% (P= 0.007). PF4618433 improved stroke volume (P= 0.031) and cardiac output (P= 0.009) in comparison to MI-vehicle with values like the Sham group. PF4618433 also led to an increase in the ejection fraction (P=0.002) and fractional shortening (P=0.006) when compared to the MI-vehicle (32% and 35% improvement, respectively) yet were lower in comparison to the Sham group. Pyk2 inhibition decreased Cx43 tyrosine phosphorylation (P=0.043) and maintained Cx43 at the intercalated disc in the distal ventricle 6-weeks post-MI.

Conclusions: Unlike other attempts to decrease Cx43 remodeling after MI induced heart failure, inhibition of Pyk2 activity maintained Cx43 at the intercalated disc. This may have aided in the reduced infarct size (acute timeframe) and improved cardiac function (chronic timeframe).

[*]To whom correspondence should be addressed: Department of Biochemistry and Molecular Biology, University of Nebraska Medical Center, Omaha, NE 68198, USA. Phone: (402) 559-7557; Fax: (402) 559-6650; psorgen@unmc.edu.

Disclosures: None

Supplemental Material
Tables S1–S6
Figure S1–S2

Additionally, we provide evidence that Pyk2 is activated following MI in human left ventricle implicating a novel potential target for therapy in patients with heart failure.

Keywords

Cx43; Pyk2; Src; phosphorylation; gap junction

Introduction

Connexin43 (Cx43), the most abundant cardiac gap junction protein, mediates ventricular propagation of cardiac action potentials and maintenance of a regular beating rhythm.[1] The importance of Cx43 gap junctions in the heart is well established: closure, dysregulation or mislocation disrupt impulse propagation, and lethal arrhythmias can ensue.[1] Following a myocardial infarction (MI; early stage-remodeling), in the surviving ventricular myocytes from the epicardial border zone, there is reduced gap junction intercellular communication (GJIC) due to changes in Cx43 expression, phosphorylation state, and membrane localization from the intercalated disc (ID) to the lateral membrane.[2, 3] An important consequence of cellular uncoupling is an increased dispersion of action potential duration and refractory period.[2] Left ventricle hypertrophy (LVH) following a MI (late-stage remodeling) is an adaptive response to increased biomechanical stress.[4] Initially, heart mass increases to normalize wall stress and retain normal cardiovascular function (compensated hypertrophy), accompanied by an increase in Cx43 expression and GJIC.[5] However, the increased cardiac mass and sustained overload eventually lead to contractile dysfunction (decompensated hypertrophy) and heart failure.[6] As LVH becomes severe, propagation velocity decreases, which correlates with reduced Cx43 expression and ID localization, as well as altered phosphorylation.[7–9]

Attempts to increase gap junction coupling in the infarct epicardial border zone have not been able to restore normal cardiac function. For example, the peptide rotigaptide partially reversed the loss of Cx43 expression in a canine model but did not affect the increase in pS368 (decreases gap junction conductance), nor prevent lateralization.[10, 11] The partial reversal of Cx43 remodeling (only expression) was not sufficient to restore normal conduction and prevent arrhythmias. In a mouse model, Src inhibitors PP1 and Saracatinib decreased Src activity to the Sham level, raised Cx43 expression at the scar border and distal ventricle, and had a higher level of the Cx43 P2 isoform (correlates with promoting GJIC).[8] Although no change in lateralization was observed, this still led to ~50% improvement in conduction velocity and lowered arrhythmia inducibility. While inhibition of Src-induced Cx43 phosphorylation could partially improve the cardiac pathology, the authors suggested that a second undiscovered process prevented full restoration of proper Cx43 function.

An *in vitro* screen identified that Pyk2 phosphorylates the carboxyl terminal domain of Cx43. Pyk2 is a Ca^{2+}-dependent nonreceptor Tyr kinase (FAK family) that transduces signals from Ca^{2+}, integrins, and G protein-coupled receptors to downstream MAPK and Akt signaling pathways.[12, 13] A series of experiments were performed to characterize this phosphorylation: 1) Cx43 and Pyk2 interact at the plasma membrane[9]; 2) Pyk2 overexpression increases Cx43 phosphorylation[9]; 3) Src activates Pyk2[9]; 4) Pyk2

phosphorylates Cx43 residues Y247, Y265, and Y313[9]; and 5) Decreasing the activation of lowers Cx43 (siRNA) tyrosine phosphorylation, without affecting the level of active Src[9]. Additionally, overexpression of Cell Adhesion Kinase-β-Related Non-kinase (endogenous Pyk2 inhibitor) improves cardiac function and slows remodeling in mouse MI models.[14] While these studies clearly show the beneficial nature of working with a Pyk2 inhibitor, a small molecule inhibitor would have a major advantage as a therapeutic for targeting Pyk2. Therefore, we worked with PF4618433, a diaryl urea small molecule inhibitor that binds Pyk2 in an allosteric binding pocket distinct from the ATP pocket to help minimizing off-target activity.[15] In comparison to classical Pyk2 inhibitors, PF4618433 had superior overall selectivity (>35 kinases tested) and improved potency to other allosteric binding pocket Pyk2 inhibitors with an IC_{50} of 637 nM.[15] To date, no studies have addressed the efficacy of using PF4618433 as a therapeutic in an animal study, which is one goal of this study.

We showed that PF4618433 inhibits Pyk2 activity in rat neonatal ventricular cardiomyocytes (NVCM), and when NVCM are PMA treated, the Pyk2 inhibitor sustains a normal beating rhythm.[9] Positive effects of the inhibitor were the result of increased Cx43 in the gap junction plaque. In the heart, Pyk2 expression is much greater in neonatal, than in adult ventricular myocytes.[16] However, animal models of heart failure and non-ischemic diseased human ventricles have identified an increase in Pyk2 expression and activity.[16–18] Revuelta-Lopez E et al. (2017) identified that at 10- and 21-days post MI, Pyk2 was activated in the peri-infarct and infarct regions, not the remote distal area.[19] In contrast, the time frame for this study is 42 days post MI, where heart failure was achieved, and activated Pyk2 was observed in the remote hypertrophy region.[9] Based upon these data, and the knowledge that phosphorylation of Y247, Y265, and Y313 blocks the Cx43 interaction with the cytoskeletal network essential for proper GJIC[20–22], we tested the hypothesis that inhibition of active Pyk2 is necessary to prevent Cx43 gap junction remodeling in MI-mediated heart failure.

Materials and Methods

The data that support the findings of this study are available from the corresponding author upon reasonable request.

Antibodies

The α-phospho-Cx43 (Y247) antibody was custom produced in rabbit from a peptide designed and chemically synthesized by LifeTein. Additional antibodies used in this study include α-Src (#2123S), α-phospho-Src (Y416) (#6943S), α-Pyk2 (#3480S), α-rabbit-Alexa488 (#4412S), α-mouse-Alexa647 (#4410S), α-rabbit-HRP (#7074), α-mouse-HRP (#7076), and GAPDH (#2118S) purchased from Cell Signaling; α-Cx43 (#13–8300) and α-phospho-Pyk2 (Y579/580) (#44–636G) purchased from ThermoFisher; α-Cx43 (#C6219) purchased from Sigma; α-phospho-Cx43 (Y265) (ab193373) and α-phospho-Pyk2 (Y402) (ab4800) purchased from Abcam. DAPI (#5748) purchased from Tocris Bioscience.

Left anterior descending artery (LAD) ligation and tissue collection

Male rats (Sprague Dawley; 200–250g) were purchased from Charles River Laboratories. All surgical procedures and animal care protocols were approved by the University of Nebraska Medical Center (UNMC) Institutional Animal Care and Use Committee and conducted according to National Institutes of Health (NIH) Guide for the Care and Use of Laboratory Animals (National Academic Press, 2011). Rats were assigned into three groups randomly: Sham control, heart failure group treated with vehicle (MI-vehicle), and heart failure group treated with PF4618433 (MI- PF4618433). Heart failure was generated by LAD ligation as previously described.[23] Briefly, rats were orally intubated and ventilated with 2–2.5% isoflurane during the surgical procedure. To produce heart failure, the LAD was ligated 1–2 mm below its origin from the aorta. The Sham group had the thoracotomy, the manipulation of the heart and lidocaine with no ligations of coronary artery. Heart failure and the degree of left ventricular dysfunction were determined by assessing morphological changes and echocardiography at the end of the experiment (6-weeks post-surgery). Rats were euthanized by pentobarbital (150 mg/kg, i.p.). Hearts were quickly removed and dissected. The left ventricle was partitioned into infarct zone, boarder zone, and remote zone for Western blot analysis or immunofluorescence staining.

We did exclude some animals in the vehicle group and PF treatment group because of the specificity of this animal model. Most of the rats were in heart failure, however a few had normal heart function (normal ejection fraction when performing the Echo and 0% infarct area after dissection). These rats were excluded. We believe the model may not have been successful due to the failure of the ligation (e.g., suture loosen).

PF4618433 treatment

One week before surgery and then for 6-weeks post-MI, the MI-PF4618433 group was injected intraperitoneally 3x a week with the Pyk2 inhibitor PF4618433 (10 μg/kg; DC Chemicals, Shanghai, China).

Echocardiography

Echocardiography was performed to determine cardiac function. Rats under light isoflurane anesthesia (1.5%) were imaged using the MX201 transducer (15 MHz) on the Vevo 3100 ultrasound machine (VisualSonics, Toronto, ON, Canada). Briefly, B-mode images were acquired in the parasternal long axis. M-mode images were acquired at the level of the left ventricular papillary muscles. Left ventricular end-diastolic diameter (LVDd) and left ventricular end-systolic diameter (LVDs) were measured. Then, ejection fraction (EF), fractional shortening (FS), left ventricular end-diastolic volume (LVd Vol), and left ventricular end-systolic volume (LVs Vol) were calculated using standard formulas from the VisualSonics VevoLab software.

Tissue collection and Western blots

Six-weeks following surgery, rats were euthanized, and hearts were excised. After excision, the atria were removed, and the ventricles were placed into a pre-chilled plate on ice. Sections were then individually examined under dissection microscope and separated into infarct zone (scar), border zone, and remote zone (distal ventricle area). Infarct zone was

identified as blanched, necrotic tissue at the anterior of the heart, consistent with a left anterior descending coronary artery occlusion. The border zone was defined as up to 2 mm of viable tissue adjacent to the edge of the infarcted tissue. Remaining viable tissue was considered remote zone. Tissues were prepared for Western blots and immunofluorescence as previously described.[9] Briefly for Western blot, tissue samples were rinsed 2x with cold 1x Tris-buffered saline (TBS) and then homogenized in lysis buffer (50 mM Tris-HCl [pH 7.4], 150 mM NaCl, 0.2% SDS, Complete protease inhibitor, and PhosSTOP) on ice for 30 min. Protein concentration was quantified by BCA assay (Pierce). A total of 30 μg protein lysate was resolved by SDS-PAGE and transferred to PVDF (EMD Millipore) membrane. Blots were blocked in 5% BSA in TBST (1x TBS, 0.1% Tween 20) for 1 hr at RT and incubated with indicated primary antibody in blocking buffer overnight at 4°C. Blots were washed 3× 10 min with TBST, and then incubated for 1 hr at RT with secondary antibody. Blots were then washed again 3× 10 min with TBST, detected using the SuperSignal West Femto Maximum Sensitivity (ThermoFisher) per manufacturer protocol, and imaged with an Invitrogen iBright Imager. Quantifications were done using NIH ImageJ software using a minimum of three independent replicates.

Immunohistochemistry

Tissue arrays of human heart samples from cardiovascular normal tissue and MI were purchased from Provitro AG, Berlin, Germany. Slides were deparaffinized in xylene and rehydrated in graded ethanol. Slides were then incubated in 0.3% hydrogen peroxide (H_2O_2) for 30 min in the dark to block endogenous peroxidase activity. After washing with TBS-T (1x TBS, 0.025% Triton), slides were microwaved 25 min for heat-induced epitope retrieval in sodium citrate buffer (10 mM sodium citrate, 0.05% Tween 20, pH 6.0). Slides were washed again with TBS-T, blocked with 2.5% horse serum for 1 hr at RT and incubated at 4°C overnight with the following primary antibody α-Pyk2 pY579/580 (1:200). The next day, sections were washed in TBS-T and incubated in HRP-conjugated horse anti-rabbit/mouse secondary antibody (Vector Laboratories #MP-7500) for 1 hr at RT. Slides were washed in TBS-T and developed using DAB peroxidase substrate kit according to manufacturer instructions (Vector Laboratories #SK4100) and counterstained with haematoxylin. Heart tissue specimens were graded according to staining intensity and percentage positive staining (1=negative; 2=weak; 3=moderate; 4=strong staining). Immunohistochemistry staining scores were analyzed and compared by one-way ANOVA and an independent t-test. All digital bright field IHC slide scanning were processed by VENTANA iScan HT (Roche) at UNMC tissue Sciences facility. The images were analyzed using Image Viewer.

Immunofluorescence

Slides were deparaffinized in xylene and rehydrated in graded ethanol. After washing with TBS-T (1x TBS, 0.025% Triton), slides were permeabilized in 50% methanol followed by heat induced epitope retrieval by microwaving for 25 min in sodium citrate buffer (10 mM sodium citrate, 0.05% Tween 20, pH 6.0). Slides were washed again with TBS-T and blocked (1x TBS with 2.5% horse serum and 0.2% Triton) for 1 hr at RT and incubated at 4°C overnight with the following primary antibodies: α-Cx43 (1:300) and α-Pyk2 pY579/580 (1:100). The next day, sections were washed 3× 10 min with 1x TBS-T,

incubated with secondary antibodies (4410S and 4412S, Cell Signaling) for 1 hr at RT, stained with DAPI (100 ng/mL) for 10 min, and then washed 3× 10 min with 1x TBS-T. Coverslips were mounted on a drop of SlowFade anti-fade (Life Tech), sealed with clear nail polish, and imaged.

Confocal imaging

All cell immunofluorescence images were acquired on a Zeiss LSM 800 Confocal system using appropriate numerical aperture objectives and appropriate filter sets.

Hematoxylin and eosin (H&E), Trichrome, and Picro Sirius Red staining of rat heart tissue

H&E staining: Slides were deparaffinized in xylene and rehydrated in graded ethanol, then incubated with H&E solutions and rinsed with water. Each slide was dehydrated through graded alcohols before being soaked in xylene twice and mounted in synthetic resin. Trichrome staining: Trichrome Stain Kit was used per manufacturer protocol (ab150686, abcam). Briefly, after deparaffination and rehydration, sections were immersed in preheat Bouin's Fluid for 1 hr at 60°C and then rinsed with tap water. Samples were then incubated for 5 min in Weigert's Iron Hematoxylin and subsequently rinsed with running tap water for 2 min. Sections were then immersed for 15 min in Biebrich Scarlet-Acid Fuchsin, differentiated in phosphomolybdic/phosphotungstic acid solution for 15 min, and incubated for 10 min in Aniline Blue solution to stain collagen fibers. Finally, samples were washed with 1% acetic acid for 5 min, dehydrated, and mounted. Picro Sirius Red staining: Picro Sirius Red Stain Kit was used per manufacturer protocol (ab150681, abcam). Briefly, slides were deparaffinized and incubated in Picro Sirius Red solution at room temperature for 1 hr. Then, the slides were washed with acetic acid, absolute alcohol, dehydrated, and mounted. After staining, collagen content was determined with digital-image microscopy with circular polarized light.

Primary cardiomyocyte isolation and quantitative mass spectrometry (MS).— Neonatal rat ventricular myocytes (NRVMs) were isolated from day 2 rat hearts using the Pierce Primary Cardiomyocyte Isolation Kit (>90% pure). Isolated NRVMs were plated at a seeding density of 2.5×10^5 cells/cm^2 in complete DMEM supplemented with 10% FBS and 1% pen-strep at 37°C in a 5% CO_2 incubator for 24 hr. The medium was then replaced with complete DMEM containing Cardiomyocyte Growth Supplement (1000X). Five days post-purification, NRVMs were pre-treated ± PF4618433 (3 hr) and then treated with PMA for 24 hrs. Samples were then provided to UNMC's MS and Proteomic Core Facility for sample processing, MS, and data analysis.

50 μg of protein per sample from four biological replicates per group was taken and detergent was removed by chloroform/methanol extraction, and the protein pellet was re-suspended in 100 mM ammonium bicarbonate and digested with MS-grade trypsin (Pierce) overnight at 37°C following reduction with 10 mM DTT at 56° C for 30 mins and alkylation using 50 mM iodoacetamide at RT for 25 mins. Peptides were cleaned with PepClean C18 spin columns (Thermo) and were re-suspended in 2% acetonitrile (ACN) and 0.1% formic acid (FA) and 500 ng of each sample was loaded onto trap column Acclaim PepMap 100 75μm × 2 cm C18 LC Columns (Thermo Scientific™) at flow rate of 4 μl/min

then separated with a Thermo RSLC Ultimate 3000 (Thermo Scientific™) on a Thermo Easy-Spray PepMap RSLC C18 75 μm × 50 cm C-18 2 μm column (Thermo Scientific™) with a step gradient of 4–25% solvent B (0.1% FA in 80 % ACN) from 10–100 min and 25–45% solvent B for 100–130 min at 300 nL/min and 50°C with a 155 min total run time. Eluted peptides were analyzed by a Thermo Orbitrap Exploris 480 (Thermo Scientific™) mass spectrometer in a data dependent acquisition mode. A survey full scan MS (from m/z 350–1200) was acquired in the Orbitrap with a resolution of 60,000. The Normalized AGC target for MS1 was set as 300% and ion filling time set as 25 ms. The most intense ions with charge state 2–6 were isolated in 3 s cycle and fragmented using HCD fragmentation with 30% normalized collision energy and detected at a mass resolution of 15,000 at 200 m/z. The AGC target for MS/MS was set as 50% and ion filling time set to auto for 30 s with a 10 ppm mass window. Protein identification was performed by searching MS/MS data against the swiss-prot Rat protein database downloaded on Nov. 2022 using the in-house PEAKS X + DB search engine. The search was set up for full tryptic peptides with a maximum of two missed cleavage sites. Acetylation of protein N-terminus and oxidized methionine were included as variable modifications and carbamidomethylation of cysteine was set as fixed modification. The precursor mass tolerance threshold was set 10 ppm for, and maximum fragment mass error was 0.02 Da. The significance threshold of the ion score was calculated based on a false discovery rate of ≤ 1%. Quantitative data analysis was performed using progenesis QI proteomics 4.2 (Nonlinear Dynamics). Statistical analysis was performed using ANOVA and The Benjamini-Hochberg method was used to adjust p-values for multiple-testing caused false discovery rate. The adjusted $p \leq 0.05$ was considered as significant. Various plots were generated using Partek Genomics Suite 7.0.

Identification of Hub genes and protein-protein interaction (PPI) network construction.—Stringdb (version 11.5) is a search tool and database for construction of PPI networks which contains experimental data. Computational prediction methods and public text data contain about 24.5 million proteins from 5,000 organisms. Hub genes, with high correlation or connectivity ranked at top 10%, were selected. By using one-way ANOVA (<0.05), differentially expressed proteins were verified in all modules. To see the protein connections, 30 hub genes were identified in which experiments contain 32 nodes and 40 edges with confidence level between the 0.400 to 0.900.

Statistical Analysis

All data were analyzed by using GraphPad Prism 8.0 and presented as the mean ± SD. Statistical analysis performed in GraphPad Prism 8.0 were either one-way ANOVA with a Neuman-Keuls post-hoc analysis or Student’s t-test where appropriate. P-values <0.05 were considered statistically significant.

Results

Pyk2 inhibitor PF4618433 is safe for animal studies.

In normal rats (no-MI), we intraperitoneally injected vehicle (propylene glycol), as well as a low (10 μg/kg) or high (40 μg/kg) dose of PF4618433 for 3 times a week for 6-weeks. At either dose, when compared to control, we observed 1) no mortality, behavioral

changes, or statistically significant difference (P>0.05) in body/organ weight (Table S1); 2) no statistically significant difference (P>0.05) in cardiac function (Table S2); 3) no statistically significant difference (P>0.05) in renal and hepatic function (Table S3); and 4) no inflammation, hemorrhaging, or tissue damage (Figure S1). Western blot analysis of left ventricular tissue after 6-weeks of treatment showed that PF4618433 decreased active Pyk2 (pY402, autophosphorylation site; pY579/580, enhances catalytic activity), and phosphorylation of Cx43 residue Y265 (targeted by Pyk2). No statistically significant difference (P>0.05) was observed in the total level of Src, active Src (p-Src), Pyk2, or Cx43 (Figure 1A and B). Since there was no statistically significant difference (P>0.05) observed between the low dose and high dose samples, the heart failure study was conducted using the low dose to decrease the probability of off target effects.

Left ventricular structure and function after MI was improved by Pyk2 inhibition.—Six-weeks post LAD ligation, rats in both the MI-vehicle and PF4618433 treated (MI-PF) groups developed anterior infarcts and heart failure (Table I); however, the presence of PF4618433 decreased the average MI infarct size from 34% to 17% (Figure 2A and B). Echocardiography data revealed that PF4618433 improved stroke volume and cardiac output in comparison to the MI-vehicle with values not statistically significant different (P>0.05) from the Sham group (Figure 3A and B). PF4618433 also led to an increase in the ejection fraction and fractional shortening when compared to the MI-vehicle (32% and 35% improvement, respectively) yet were significantly reduced in comparison to the Sham group. The difference between the MI-vehicle and MI-PF groups in the infarct size and left ventricle function suggest that inhibiting Pyk2 could have a beneficial effect towards decreasing heart failure.

Pyk2 was activated following MI and inhibited by PF4618433 treatment.—There was no change in the total protein level of Pyk2 between the Sham, MI-vehicle, and MI-PF groups in the distal left ventricle of the heart 6-weeks post LAD ligation (Figure 4A and B). In the MI-vehicle group, phosphorylation of Pyk2 residue Y402 increased by 89% and phosphorylation of Pyk2 residues Y579 and Y580 increased by 65%. PF4618433 treatment prevented the increase in Pyk2 activation following the MI and showed no statistically significant difference (P>0.05 for all) from the Sham group.

Pyk2 inhibition decreased the level of Cx43 phosphorylation following MI.—6-weeks post LAD ligation, no change in the level of Cx43 was observed between the Sham and MI groups (Figure 4A and B). In the distal left ventricle, the MI-vehicle had a 100% increase in the level of phosphorylation at Cx43 residues Y247. This increase was completely reversed by treatment with PF4618433. Since inhibiting phosphorylation of these Pyk2 sites improves GJIC[9], the data suggests if Cx43 is maintained at the intercalated disc as opposed to the lateral membrane, this would improve impulse propagation.

Pyk2 inhibition maintains Cx43 at the intercalated disc following MI.—Immunofluorescence images (longitudinal sections) of the distal left ventricle show Cx43 only at the intercalated disc in the Sham group and Cx43 at the intercalated disc and lateral membrane in the MI-vehicle (Figure 5A and B). While there was little-to-no active Pyk2 in

the Sham group, the increase in active Pyk2 following the MI was colocalized with Cx43 in the MI-vehicle. Interestingly, treatment with PF4618433 not only decreased the level of active Pyk2 compared to the MI-vehicle, but Cx43 was maintained at the intercalated disc following the MI.

Pyk2 was activated following MI in human left ventricle.—Our data indicate in a rat model of heart failure that Pyk2 is activated in the left ventricle. However, Lang et al 2011 provided Western blot data from diseased human left ventricle caused by a MI and found no activation of Pyk2.[18] Therefore, we analyzed a tissue array that contains 24 heart samples (4 normal tissue, 8 granulation tissue; 10–14 days post-MI; healing of inflammation involving ingrowth of capillaries and accompanied by fibroblasts producing collagen, and 12 scar tissue; >2 months post-MI; accumulation of fibrous tissue replacement of necrotic or extensively damaged tissue) in both the longitudinal and transverse sections (Figure 6 and Figure S2). In the normal tissue, there is little-to-no activated Pyk2 (pY579/pY580). Conversely, there is a significant increase in the level of activated Pyk2 in the remaining cardiomyocytes in the granulation and scar tissues. These data, along with the benefits observed from inhibiting Pyk2 activity in the MI animal model, suggests PF4618433 has the potential to be translatable to the human cardiac disease.

Potential mechanisms of PF4618433 and Pyk2 inhibition.—To gain an initial understanding of how inhibition of Pyk2 is causing these beneficial changes in this post-MI heart failure model, we performed MS-based proteomics using purified NRVMs. When compared to the control (no PMA), the presence of PMA significantly (p-value <0.05) affected 314 genes (Table S4). Of these genes, the three most significantly affected cardiac biological processes include cardiac muscle cell development (Sorbs2, Myh11, Pdlim5; p-value 3.32 E-07), heart development (Ndrg4, Pdlim5, Crip1; p-value 1.13 E-04), and ventricular cardiac muscle tissue morphogenesis (Smad4, Eng; p-value 1.83E-04). The presence of PF4618433 (PMA_PF vs. PMA) affected 653 genes (Table S5). Of these genes, the three most significantly affected cardiac biological processes include heart development (Pdlim1, Cdkn1A, Sgcd, Casp8, Cxadr, Pkp2, Gata4, Tnni3, Ptk2; p-value 3.72 E-13), negative regulation of cardiac muscle hypertrophy (Mlip, Smad4, P2rx4, Cav3, Atp2b4; p-value 1.94 E-12), and cardiac muscle tissue development (Notch2, Smad4, Sgcd, Nppa, Ankrd1, Gata4; p-value 5.71 E-11). In comparing the two lists, the presence of PF4618433 reversed a total of six genes from PMA only, all to the downside (Smad4, Xrn1, Renbp, Dynll1, Enpp1, 0 β−2 Globin). We also compared the PMA_PF to control data sets and found 632 affected genes (Table S6).

In both the PMA and PMA_PF data sets, the level of Pyk2 gene (Ptk2b) expression was not affected. This is consistent with a previous PMA study which showed no change in the protein level of Pyk2[9] as well as there was no change of Pyk2 in the post-MI failing heart (Figure 4). Since highly connected hub nodes are central to a network's architecture and function, we artificially added Ptk2b into the genes significantly affected when comparing the data sets (control, PMA, and PMA_PF) to identify the genes most likely affected by inhibiting Pyk2 (Figure 7A). While several affected genes are a part of the focal adhesion molecular architecture (Pxn, Actn4, Itgb1, Tns1, Vcl, Grb2, Src), a number were not

(Sirpa, Capn2, Epha2). To provide evidence that this proteomic study has the potential to provide future avenues of study to help mechanistically explain the beneficial effects of PF4618433 in the post-MI heart, we independently tested the impact of PF4618433 on a highly confident affected connection, that between Pyk2 and Paxillin (Figure 7B). Using Cx43 over-expressing HeLa cells, increasing concentrations of PF4618433 counteracted the effect of PMA by returning active Paxillin to the pre-PMA active level (concentration of PF4618433; 25 μM).

Discussion

Mechanisms underlying the initiation and persistence of lethal cardiac rhythms are of significant clinical interest. Therefore, knowing what causes these alterations is essential to define the pathological cellular substrate and devise effective therapies. Whether in the surviving ventricular myocytes from the epicardial border zone or in decompensated hypertrophy and heart failure, the cardiac muscle sarcoplasm experiences many abnormalities; including reduced GJIC due to changes in Cx43 expression and increased relocalization from the ID to lateral membrane.[3, 24–26] One mechanism for these alterations is a change in the Cx43 phosphorylation state. Phosphorylation at S325, S328, and S330 by Casein Kinase 1 is necessary for assembly of gap junction plaques, and phosphorylation at S365 by PKA is important for trafficking to the plasma membrane (for review see[27]). These sites have been implicated in pathogenesis because their phosphorylation status is altered during acute ischemia and heart failure, leading to a decrease of Cx43 at the ID. For example, mice in which S325/328/330 are mutated to alanine's display disturbed gap junction formation and are susceptible to arrhythmias.[28] Cx43 phosphorylation on S279/S282 decreases GJIC through clathrin-mediated endocytosis.[29] One additional site, S368, which becomes phosphorylated during cellular stress, may lead to a decrease in gap junction conductance.[10, 30] Additionally, Freitas-Andrade et al. (2019) used a knock-in Cx43 with serine to alanine mutations at the MAPK sites $Cx43^{S255/262/279/282A}$ on a permanent middle cerebral artery occlusion stroke model.[31] They demonstrated that these transgenic animals exhibit a significant decrease in infarct volume, potentially via reduced Cx43 hemichannel activity. Thus, we speculate based upon these data that any mechanism by which Cx43 is preserved at the ID in a form able to permit proper GJIC would be beneficial towards reducing infarct size and increasing ventricular contractile function.

While Cx43 lateralization is an almost ubiquitous response to cardiac pathology[2, 32, 33], the molecular mechanisms of this remodeling are unknown. Based upon prior mechanistic studies[9, 20–22, 34], we propose a model for Cx43 ID localization which involves Pyk2 and Src disrupting the interaction between Cx43 and the cytoskeletal network. First, activation of Src leads to activation of Pyk2 and subsequent translocation to gap junctions at the ID, where Pyk2 phosphorylates Cx43CT residues Y247, Y265, and Y313.[9, 35, 36] pY247 inhibits the Cx43 interaction with β-tubulin[21], pY265 and pY313 inhibit the interaction with Drebrin (binds F-actin)[20, 22], and Src interacts with ZO-1 (binds F-actin) causing ZO-1 displacement from the Cx43CT.[3] Once ZO-1 unhooks, the plaque size increases[37], but as it is no longer anchored at the ID (also caused by loss of interaction with tubulin and Drebrin), Cx43 moves away from the region of high concentration at the ID to the lateral membrane.

Consistent with this hypothesis is that the lateralized gap junctions are in larger than normal plaques.[38] We have shown that by one hour-post LAD ligation in a canine model, there is no Cx43 co-localization with ZO-1 in the epicardial border zone myocytes, and after three hours the entire lateral membrane is covered with Cx43.[3] Another noticeable change was the increase in the interaction of active Src with ZO-1 at 30 minutes post LAD ligation that further increased over the three hours.[3]

Rutledge et al (2014) evaluated the role of Src inhibition on Cx43 regulation in a mouse model of MI.[8] Src inhibition improved conduction velocity and reduced arrhythmia inducibility, however no change was observed in the infarct size or cardiac function. While overall Cx43 expression increased, immunohistochemistry staining showed no evidence of improvement in Cx43 lateralization with Src inhibition. Conversely, PF4618433 treatment blocked Cx43 lateralization, reduced infarct size, and improved cardiac function. We speculate these improvements were the result of maintaining Cx43 at the ID. Support for this prospect comes from an adenoviral-induced expression study, which increased Cx43 at the ID in the infarct epicardial border zone, improved conduction velocity, and reduced arrhythmia susceptibility[39], however there was no improvement in the degree of lateralization (ID/lateral membrane ratio). While this study focused on LVH, studies have shown that Pyk2 can be directly activated by acidic pH as what occurs in the surviving myocytes at the epicardial border zone.[40] The data suggest that any targeted mechanism that can increase the Cx43 ID/lateral membrane ratio under endogenously expressing conditions would be therapeutically beneficial. Using the knowledge of how Src interacts and phosphorylates Pyk2 and Cx43, we identified that Pyk2 has a greater impact on Cx43 phosphorylation than Src.[9] Thus, the possibility exists that Pyk2 remained active in the Rutledge et al (2014) study based upon incomplete inhibition of Src by PP1[8], activation by another Src family member[41], or activation via a Src-independent mechanism.[16, 40]

Because Pyk2 activates MAPK and Akt[12, 13], benefits of inhibiting Pyk2 would also include decreased phosphorylation of Cx43 residues S279 and S282 (MAPK sites; phosphorylation channel open probability and possibly altered selectivity[42]) and S373 (Akt site; phosphorylation inhibits ZO-1 interaction with Cx43). Of note, although S373 phosphorylation initially increases plaque size and GJIC, the increased size may contribute to more efficient internalization of gap junctions.[43] In addition to these favorable outcomes towards promoting Cx43 GJIC, one cannot discard possible changes in the phosphorylation state of other substrates of Pyk2 that may in turn influence infarct size and/or cardiac function. These would include maintaining myofibril organization and decreasing apoptotic signaling via paxillin[44], improving contractions by normalizing expression of SERCA2[45], reducing infarct size via eNOS[46], and decreasing left ventricle remodeling by inhibiting MMP-9 activation.[19]

In summary, unlike other attempts to decrease Cx43 remodeling after a MI, inhibition of Pyk2 activity by PF4618433 maintained Cx43 localization to the intercalated disc. After acute MI this may have aided in reducing the infarct size, and this along with improved myocyte communication distal to the infarct in the LVH, may have been responsible for the improved cardiac function. Our data suggest that Cx43 tyrosine phosphorylation after MI is driven by Pyk2, not Src, as only inhibition of Pyk2 maintained localization of Cx43

to the intercalated disc. Additionally, we provide the first evidence that Pyk2 is activated following MI in human left ventricle. While this study focused on addressing if 1) inhibiting Pyk2 would improve cardiac function after a MI and 2) if one mechanism for this beneficial effect is via Cx43, future studies will explore the impact of Pyk2 inhibition on fibrosis, inflammation, and arrhythmias following MI.

Limitations of this study.

1) Off target effects: Inhibition of Pyk2 activity will undoubtedly directly affect targets other than Cx43. Additionally, while PF4618433 is relatively specific for Pyk2, it could affect other tyrosine kianses.[15] The MS-based proteomics approach was utilized to help address these concerns. 2) Dosage regiment: The goal of this study was to identify if inhibition of Pyk2 would have any beneficial effect in a MI-model of heart failure. Therefore, the experimental design was tailored towards this goal (i.e., 7-week treatments commencing 1-week prior to the ligation plus 6-weeks post MI) and not what would be optimal for human treatment. The injections were done 3 times a week, therefore the possibility exists that Pyk2 inhibition varies over the dosing schedule. The 7-week treatments are significantly longer than the half-life of Cx43 (only a few hours), which does not allow for discerning acute vs. chronic affects. Also, the effects of Src and Pyk2 are difficult to disentangle over this period. 3) Although we would have preferred to investigate all three Src phosphorylation sites on Cx43, unfortunately during this study the pY247 antibody was no longer commercially available and the pY313 antibody was no longer viable.

Supplementary Material

Refer to Web version on PubMed Central for supplementary material.

Acknowledgments:

We would like to thank the University of Nebraska Medical Center Small Animal Ultrasound Core Facility for helping with echocardiography Imaging and analysis. We would also like to thank the Advanced Microscopy Core Facility at the University of Nebraska Medical Center for helping with confocal microscopy. The University of Nebraska Medical Center Mass Spectrometry and Proteomics Core Facility is administrated through the Office of the Vice Chancellor for Research and supported by state funds from the Nebraska Research Initiative.

Sources of Funding:

This work was supported by a grant from the NIH (GM072631) to P. L. Sorgen and a NIH (R01-DK-114663) grant and endowed McIntyre Professorship to K.P. Patel. Support for the UNMC Advanced Microscopy Core Facility was provided by the Nebraska Research Initiative and an Institutional Development Award from the NIH (P30GM106397). The following NIH SIG funded instruments were used: LSM 800 Zeiss Confocal Microscope (NIH S10RR027301). The UNMC-Small Animal Ultrasound Core is supported in part by funding from the Nebraska Center for Nanomedicine COBRE grant, NIGMS P30 GM127200.

Nonstandard Abbreviations and Acronyms:

MI	Myocardial infarction
Cx43	Connexin43
GJIC	Gap junction intercellular communication
ID	Intercalated disc

LVH	Left ventricle hypertrophy
NVCM	Rat neonatal ventricular cardiomyocytes
H&E	Hematoxylin and eosin
ACN	Acetonitrile
LAD	Left anterior descending artery
FA	Formic acid
PPI	Protein-protein interaction
PF	PF4618433

References

1. Severs NJ, Bruce AF, Dupont E and Rothery S. Remodelling of gap junctions and connexin expression in diseased myocardium. Cardiovasc Res. 2008;80:9–19. [PubMed: 18519446]
2. Peters NS, Coromilas J, Severs NJ and Wit AL. Disturbed connexin43 gap junction distribution correlates with the location of reentrant circuits in the epicardial border zone of healing canine infarcts that cause ventricular tachycardia. Circulation. 1997;95:988–96. [PubMed: 9054762]
3. Kieken F, Mutsaers N, Dolmatova E, Virgil K, Wit AL, Kellezi A, Hirst-Jensen BJ, Duffy HS and Sorgen PL. Structural and molecular mechanisms of gap junction remodeling in epicardial border zone myocytes following myocardial infarction. Circ Res. 2009;104:1103–12. [PubMed: 19342602]
4. Frey N, Katus HA, Olson EN and Hill JA. Hypertrophy of the heart: a new therapeutic target? Circulation. 2004;109:1580–9. [PubMed: 15066961]
5. Jin H, Chemaly ER, Lee A, Kho C, Hadri L, Hajjar RJ and Akar FG. Mechanoelectrical remodeling and arrhythmias during progression of hypertrophy. FASEB J. 2010;24:451–63. [PubMed: 19825979]
6. Shiojima I, Sato K, Izumiya Y, Schiekofer S, Ito M, Liao R, Colucci WS and Walsh K. Disruption of coordinated cardiac hypertrophy and angiogenesis contributes to the transition to heart failure. J Clin Invest. 2005;115:2108–18. [PubMed: 16075055]
7. Cooklin M, Wallis WR, Sheridan DJ and Fry CH. Changes in cell-to-cell electrical coupling associated with left ventricular hypertrophy. Circ Res. 1997;80:765–71. [PubMed: 9168778]
8. Rutledge CA, Ng FS, Sulkin MS, Greener ID, Sergeyenko AM, Liu H, Gemel J, Beyer EC, Sovari AA, Efimov IR and Dudley SC. c-Src kinase inhibition reduces arrhythmia inducibility and connexin43 dysregulation after myocardial infarction. J Am Coll Cardiol. 2014;63:928–34. [PubMed: 24361364]
9. Zheng L, Trease AJ, Katsurada K, Spagnol G, Li H, Shi W, Duan B, Patel KP and Sorgen PL. Inhibition of Pyk2 and Src activity improves Cx43 gap junction intercellular communication. J Mol Cell Cardiol. 2020;149:27–40. [PubMed: 32956670]
10. Ek-Vitorin JF, King TJ, Heyman NS, Lampe PD and Burt JM. Selectivity of connexin 43 channels is regulated through protein kinase C-dependent phosphorylation. Circ Res. 2006;98:1498–505. [PubMed: 16709897]
11. Macia E, Dolmatova E, Cabo C, Sosinsky AZ, Dun W, Coromilas J, Ciaccio EJ, Boyden PA, Wit AL and Duffy HS. Characterization of gap junction remodeling in epicardial border zone of healing canine infarcts and electrophysiological effects of partial reversal by rotigaptide. Circ Arrhythm Electrophysiol. 2011;4:344–51. [PubMed: 21493965]
12. Blaukat A, Ivankovic-Dikic I, Gronroos E, Dolfi F, Tokiwa G, Vuori K and Dikic I. Adaptor proteins Grb2 and Crk couple Pyk2 with activation of specific mitogen-activated protein kinase cascades. J Biol Chem. 1999;274:14893–901. [PubMed: 10329689]

13. Guo J, Sabri A, Elouardighi H, Rybin V and Steinberg SF. Alpha1-adrenergic receptors activate AKT via a Pyk2/PDK-1 pathway that is tonically inhibited by novel protein kinase C isoforms in cardiomyocytes. Circ Res. 2006;99:1367–75. [PubMed: 17110596]

14. Koshman YE, Chu M, Kim T, Kalmanson O, Farjah M, Kumar M, Lewis W, Geenen DL, de Tombe P, Goldspink PH, Solaro RJ and Samarel AM. Cardiomyocyte-specific expression of CRNK, the C-terminal domain of PYK2, maintains ventricular function and slows ventricular remodeling in a mouse model of dilated cardiomyopathy. J Mol Cell Cardiol. 2014;72:281–91. [PubMed: 24713463]

15. Han S, Mistry A, Chang JS, Cunningham D, Griffor M, Bonnette PC, Wang H, Chrunyk BA, Aspnes GE, Walker DP, Brosius AD and Buckbinder L. Structural characterization of proline-rich tyrosine kinase 2 (PYK2) reveals a unique (DFG-out) conformation and enables inhibitor design. J Biol Chem. 2009;284:13193–201. [PubMed: 19244237]

16. Bayer AL, Heidkamp MC, Howes AL, Heller Brown J, Byron KL and Samarel AM. Protein kinase C epsilon-dependent activation of proline-rich tyrosine kinase 2 in neonatal rat ventricular myocytes. J Mol Cell Cardiol. 2003;35:1121–33. [PubMed: 12967635]

17. Melendez J, Welch S, Schaefer E, Moravec CS, Avraham S, Avraham H and Sussman MA. Activation of pyk2/related focal adhesion tyrosine kinase and focal adhesion kinase in cardiac remodeling. J Biol Chem. 2002;277:45203–10. [PubMed: 12228222]

18. Lang D, Glukhov AV, Efimova T and Efimov IR. Role of Pyk2 in cardiac arrhythmogenesis. Am J Physiol Heart Circ Physiol. 2011;301:H975–83. [PubMed: 21666110]

19. Revuelta-Lopez E, Soler-Botija C, Nasarre L, Benitez-Amaro A, de Gonzalo-Calvo D, Bayes-Genis A and Llorente-Cortes V. Relationship among LRP1 expression, Pyk2 phosphorylation and MMP-9 activation in left ventricular remodelling after myocardial infarction. J Cell Mol Med. 2017;21:1915–1928. [PubMed: 28378397]

20. Zheng L, Li H, Cannon A, Trease AJ, Spagnol G, Zheng H, Radio S, Patel K, Batra S and Sorgen PL. Phosphorylation of Cx43 residue Y313 by Src contributes to blocking the interaction with Drebrin and disassembling gap junctions. J Mol Cell Cardiol. 2019;126:36–49. [PubMed: 30448479]

21. Saidi Brikci-Nigassa A, Clement MJ, Ha-Duong T, Adjadj E, Ziani L, Pastre D, Curmi PA and Savarin P. Phosphorylation controls the interaction of the connexin43 C-terminal domain with tubulin and microtubules. Biochemistry. 2012;51:4331–42. [PubMed: 22558917]

22. Ambrosi C, Ren C, Spagnol G, Cavin G, Cone A, Grintsevich EE, Sosinsky GE and Sorgen PL. Connexin43 Forms Supramolecular Complexes through Non-Overlapping Binding Sites for Drebrin, Tubulin, and ZO-1. PLoS One. 2016;11:e0157073. [PubMed: 27280719]

23. Patel KP, Zhang PL and Carmines PK. Neural influences on renal responses to acute volume expansion in rats with heart failure. Am J Physiol. 1996;271:H1441–8. [PubMed: 8897938]

24. Turner MS, Haywood GA, Andreka P, You L, Martin PE, Evans WH, Webster KA and Bishopric NH. Reversible connexin 43 dephosphorylation during hypoxia and reoxygenation is linked to cellular ATP levels. Circ Res. 2004;95:726–33. [PubMed: 15358666]

25. Lampe PD, Cooper CD, King TJ and Burt JM. Analysis of Connexin43 phosphorylated at S325, S328 and S330 in normoxic and ischemic heart. J Cell Sci. 2006;119:3435–42. [PubMed: 16882687]

26. Hamilton S, Terentyeva R, Clements RT, Belevych AE and Terentyev D. Sarcoplasmic reticulum-mitochondria communication; implications for cardiac arrhythmia. J Mol Cell Cardiol. 2021;156:105–113. [PubMed: 33857485]

27. Sorgen PL, Trease AJ, Spagnol G, Delmar M and Nielsen MS. Protein(−)Protein Interactions with Connexin 43: Regulation and Function. Int J Mol Sci. 2018;19. [PubMed: 30577572]

28. Remo BF, Qu J, Volpicelli FM, Giovannone S, Shin D, Lader J, Liu FY, Zhang J, Lent DS, Morley GE and Fishman GI. Phosphatase-resistant gap junctions inhibit pathological remodeling and prevent arrhythmias. Circ Res. 2011;108:1459–66. [PubMed: 21527737]

29. Johnson KE, Mitra S, Katoch P, Kelsey LS, Johnson KR and Mehta PP. Phosphorylation on Ser-279 and Ser-282 of connexin43 regulates endocytosis and gap junction assembly in pancreatic cancer cells. Mol Biol Cell. 2013;24:715–33. [PubMed: 23363606]

30. Lampe PD, TenBroek EM, Burt JM, Kurata WE, Johnson RG and Lau AF. Phosphorylation of connexin43 on serine368 by protein kinase C regulates gap junctional communication. J Cell Biol. 2000;149:1503–12. [PubMed: 10871288]

31. Freitas-Andrade M, Wang N, Bechberger JF, De Bock M, Lampe PD, Leybaert L and Naus CC. Targeting MAPK phosphorylation of Connexin43 provides neuroprotection in stroke. J Exp Med. 2019;216:916–935. [PubMed: 30872361]

32. Akar FG, Nass RD, Hahn S, Cingolani E, Shah M, Hesketh GG, DiSilvestre D, Tunin RS, Kass DA and Tomaselli GF. Dynamic changes in conduction velocity and gap junction properties during development of pacing-induced heart failure. Am J Physiol Heart Circ Physiol. 2007;293:H1223–30. [PubMed: 17434978]

33. Kaplan SR, Gard JJ, Protonotarios N, Tsatsopoulou A, Spiliopoulou C, Anastasakis A, Squarcioni CP, McKenna WJ, Thiene G, Basso C, Brousse N, Fontaine G and Saffitz JE. Remodeling of myocyte gap junctions in arrhythmogenic right ventricular cardiomyopathy due to a deletion in plakoglobin (Naxos disease). Heart Rhythm. 2004;1:3–11. [PubMed: 15851108]

34. Sorgen PL, Duffy HS, Sahoo P, Coombs W, Delmar M and Spray DC. Structural changes in the carboxyl terminus of the gap junction protein connexin43 indicates signaling between binding domains for c-Src and zonula occludens-1. J Biol Chem. 2004;279:54695–701. [PubMed: 15492000]

35. Seko Y, Tobe K, Takahashi N, Kaburagi Y, Kadowaki T and Yazaki Y. Hypoxia and hypoxia/reoxygenation activate Src family tyrosine kinases and p21ras in cultured rat cardiac myocytes. Biochem Biophys Res Commun. 1996;226:530–5. [PubMed: 8806668]

36. Yamaji Y, Tsuganezawa H, Moe OW and Alpern RJ. Intracellular acidosis activates c-Src. Am J Physiol. 1997;272:C886–93. [PubMed: 9124524]

37. Hunter AW, Barker RJ, Zhu C and Gourdie RG. Zonula occludens-1 alters connexin43 gap junction size and organization by influencing channel accretion. Mol Biol Cell. 2005;16:5686–98. [PubMed: 16195341]

38. Cabo C, Yao J, Boyden PA, Chen S, Hussain W, Duffy HS, Ciaccio EJ, Peters NS and Wit AL. Heterogeneous gap junction remodeling in reentrant circuits in the epicardial border zone of the healing canine infarct. Cardiovasc Res. 2006;72:241–9. [PubMed: 16914125]

39. Greener ID, Sasano T, Wan X, Igarashi T, Strom M, Rosenbaum DS and Donahue JK. Connexin43 gene transfer reduces ventricular tachycardia susceptibility after myocardial infarction. J Am Coll Cardiol. 2012;60:1103–10. [PubMed: 22883636]

40. Li S, Sato S, Yang X, Preisig PA and Alpern RJ. Pyk2 activation is integral to acid stimulation of sodium/hydrogen exchanger 3. J Clin Invest. 2004;114:1782–9. [PubMed: 15599403]

41. Canino J, Guidetti GF, Galgano L, Vismara M, Minetti G, Torti M and Canobbio I. The proline-rich tyrosine kinase Pyk2 modulates integrin-mediated neutrophil adhesion and reactive oxygen species generation. Biochim Biophys Acta Mol Cell Res. 2020;1867:118799. [PubMed: 32693110]

42. Cottrell GT, Lin R, Warn-Cramer BJ, Lau AF and Burt JM. Mechanism of v-Src- and mitogen-activated protein kinase-induced reduction of gap junction communication. Am J Physiol Cell Physiol. 2003;284:C511–20. [PubMed: 12388103]

43. Solan JL and Lampe PD. Specific Cx43 phosphorylation events regulate gap junction turnover in vivo. FEBS Lett. 2014;588:1423–9. [PubMed: 24508467]

44. Melendez J, Turner C, Avraham H, Steinberg SF, Schaefer E and Sussman MA. Cardiomyocyte apoptosis triggered by RAFTK/pyk2 via Src kinase is antagonized by paxillin. J Biol Chem. 2004;279:53516–23. [PubMed: 15322113]

45. Heidkamp MC, Scully BT, Vijayan K, Engman SJ, Szotek EL and Samarel AM. PYK2 regulates SERCA2 gene expression in neonatal rat ventricular myocytes. Am J Physiol Cell Physiol. 2005;289:C471–82. [PubMed: 15829561]

46. Bibli SI, Zhou Z, Zukunft S, Fisslthaler B, Andreadou I, Szabo C, Brouckaert P, Fleming I and Papapetropoulos A. Tyrosine phosphorylation of eNOS regulates myocardial survival after an ischaemic insult: role of PYK2. Cardiovasc Res. 2017;113:926–937. [PubMed: 28444132]

What is New?

- Myocardial infarction activated Pyk2 in the left ventricle causes altered phosphorylation and function of Connexin43.
- Pyk2 inhibitor PF4618433 has a therapeutic effect on cardiac function in myocardial infarction rats (decreased infract size and improved cardiac function), in part, by preventing Cx43 lateralization in the left ventricle.

What are the clinical implications?

- Changes in Connexin43 distribution, density, and channel properties are characteristic of arrhythmic heart disease. Therefore, knowing what causes these alterations is essential to define the pathological cellular substrate and devise effective therapies.
- Pyk2 is activated following myocardial infarction in human left ventricle implicating a novel potential target for therapy in patients with heart failure.

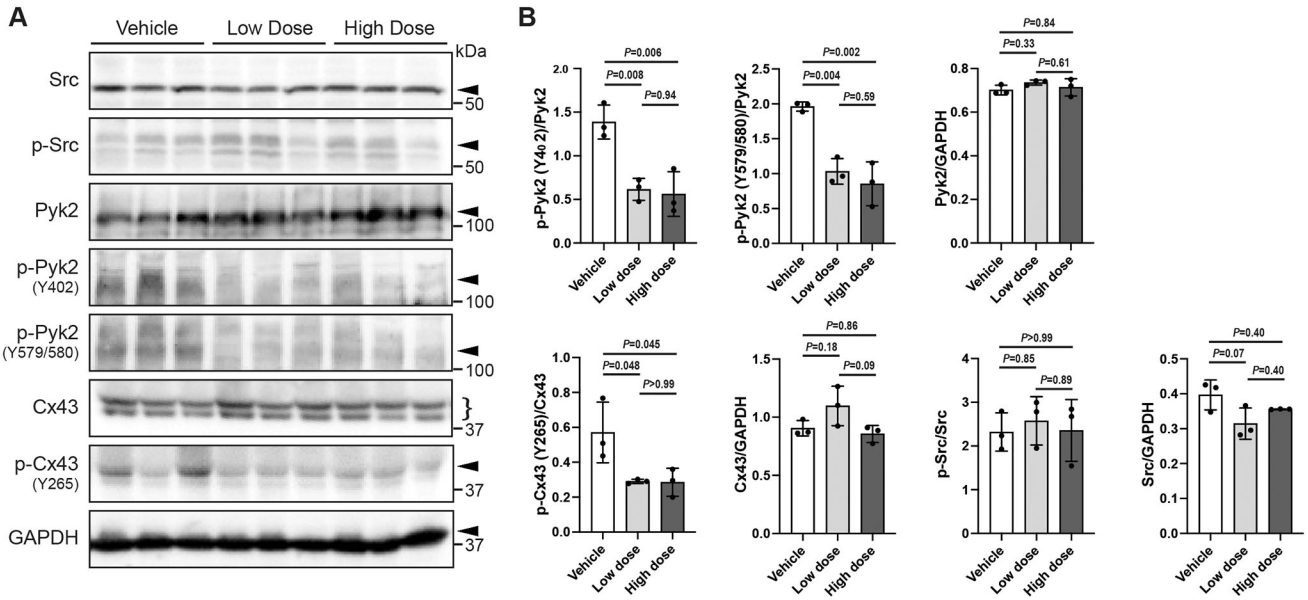

Figure 1. Effect of PF4618433 on the level of active Pyk2 and Connexin43 phosphorylation in the heart.

Left ventricle tissue lysate from rats 6-weeks post treatment with low (10 μg/kg) or high (40 μg/kg) dose of PF4618433 were compared with the control (Vehicle only) via Western blotting. A) Shown are representative images from 3 different samples from each group. Antibodies used are labeled on the left of each panel. The arrow is pointing at the molecular mass of the protein. For Connexin43 (Cx43), a bracket is displayed because of the different electrophoretic isoforms when run on a SDS-PAGE. B) Protein levels were quantified by analyzing scanned blots using ImageJ software. Phosphorylated protein levels were normalized to total protein. Data are representative of three independent experiments (one-way ANOVA, p-values have been provided). Vehicle, n=5; Low Dose, n=5, High Dose, n=5.

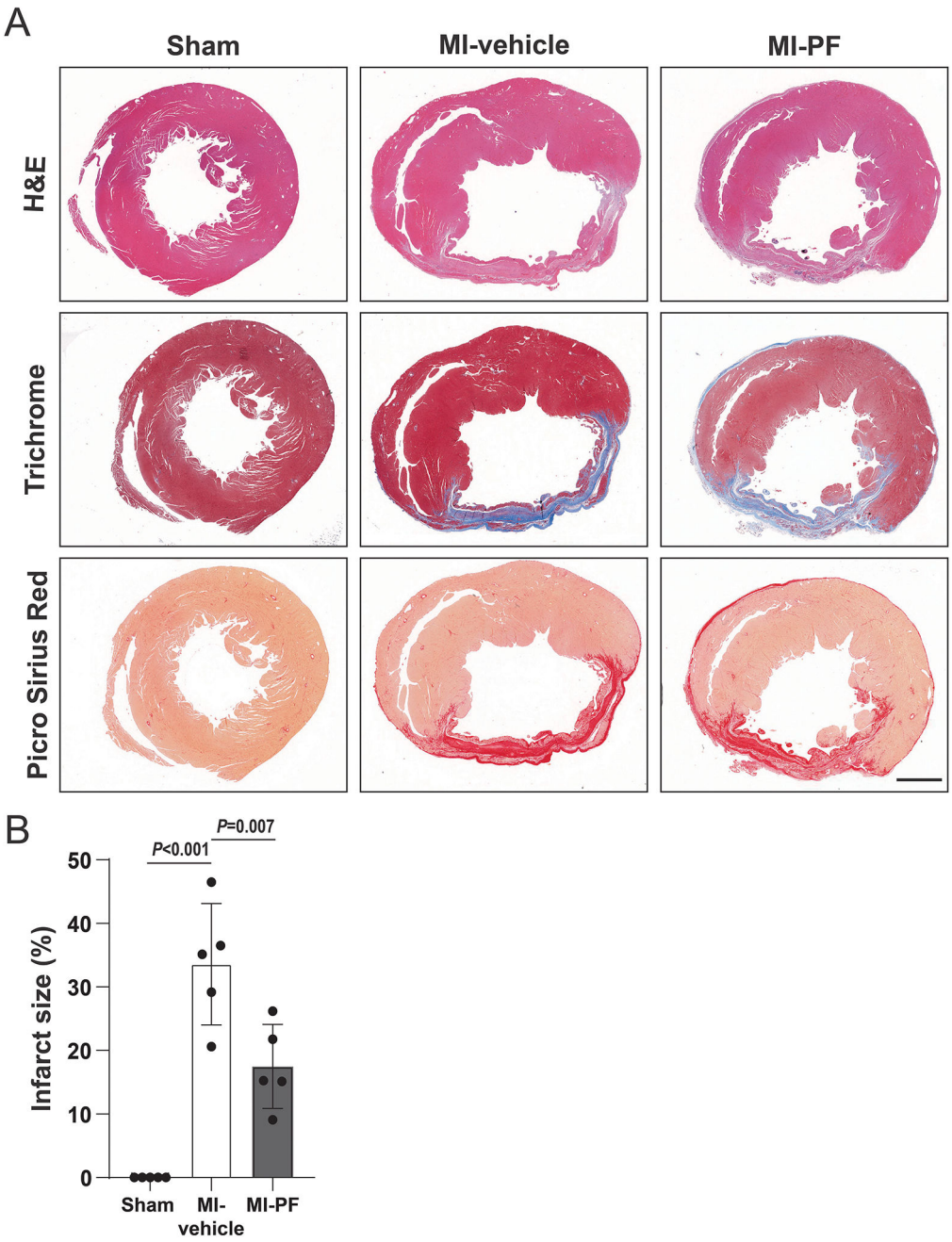

Figure 2. Histological evaluation of hearts to determine infarct size after PF4618433 treatment in myocardial infarction rats.

Six-weeks after Sham or left anterior descending artery ligation (treated with or without PF4618433 (PF)), rat hearts were harvested for (A) Hematoxylin and eosin (H&E) staining, Masson's trichrome staining of collagen fibers (blue), and Picro Sirius Red staining of collagen fibers (red). B) Quantification of fibrosis area (one-way ANOVA, p-values have been provided). Sham, n=5; Myocardial infarction (MI)-vehicle, n=5, MI-PF, n=8. Scale bar = 2 mm.

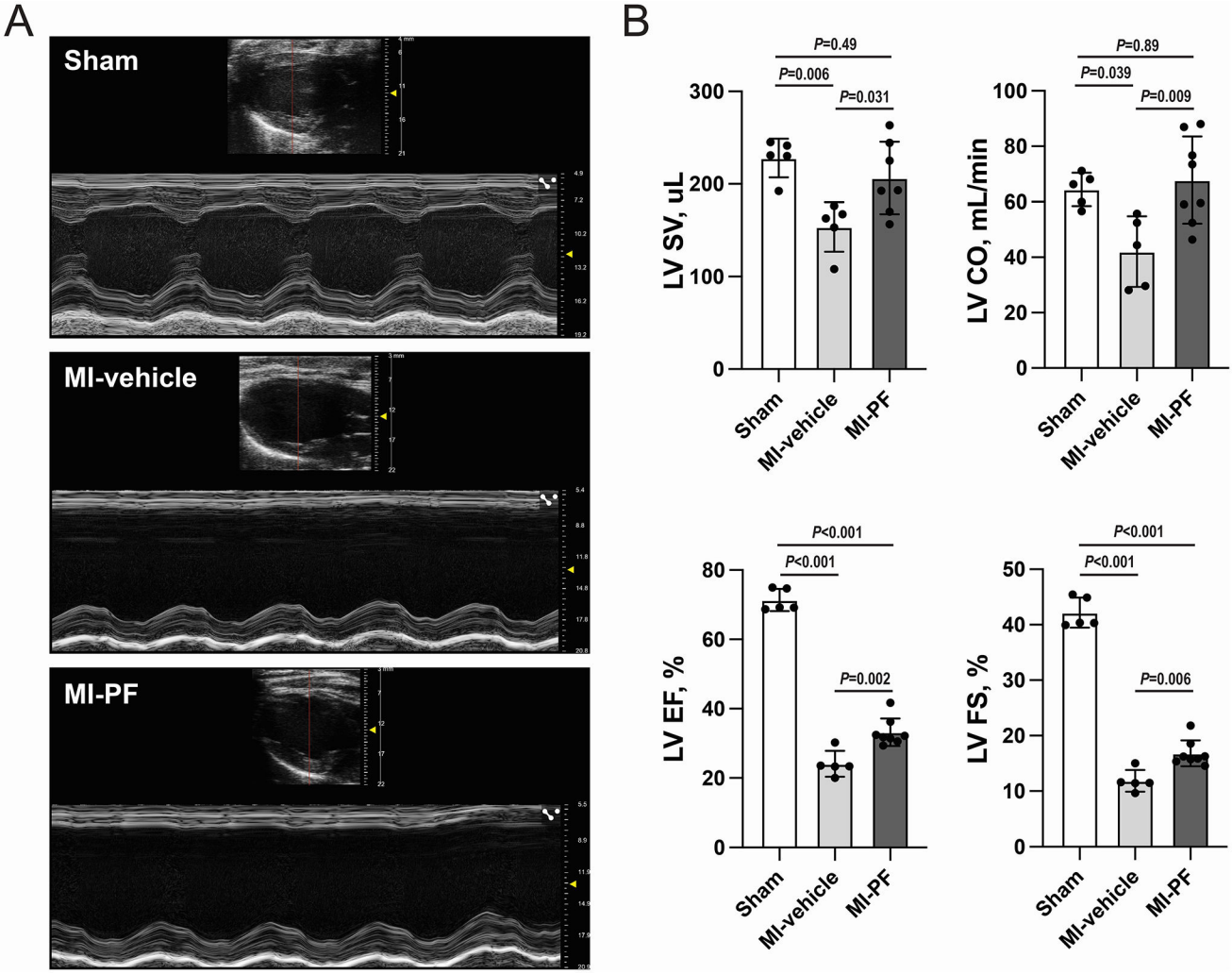

Figure 3. Cardiac function detected by echocardiography after PF4618433 treatment in myocardial infarction rats.

A) Representative M-mode echocardiographic images six-weeks after Sham or left anterior descending artery ligation treated without (Myocardial infarction (MI)-vehicle) or with PF4618433 (MI-PF). The red lines indicate the cross section for measurement. B) Quantification of Stroke volume (SV), Cardiac output (CO), LV ejection fraction (LVEF), and Fractional shortening (LVFS) (one-way ANOVA, p-values have been provided). Sham, n=5; MI-vehicle, n=5, MI-PF, n=8.

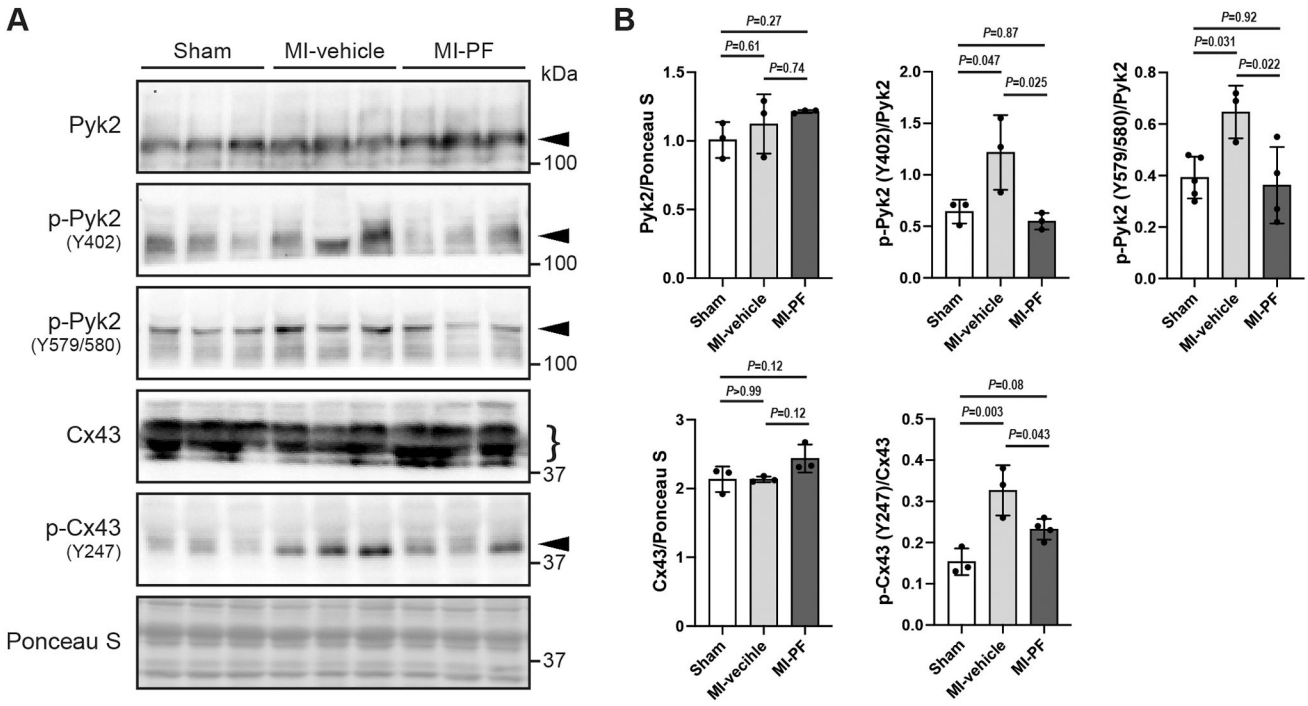

Figure 4. Effect of PF4618433 on the level of active Pyk2 and Connexin43 phosphorylation in the myocardial infarction rat heart.

Left ventricle tissue lysate (distal to the infarction, hypertrophy area) from 6-weeks after Sham or left anterior descending artery ligation treated without (Myocardial infarction (MI)-vehicle) or with PF4618433 (MI-PF) were compared via Western blotting. A) Shown are representative blots from 3 different samples from each group. Antibodies used are labeled on the left of each panel. The arrow is pointing at the molecular mass of the protein. For Connexin43 (Cx43), a bracket is displayed because of the different electrophoretic isoforms when run on a SDS-PAGE. B) Protein levels were quantified by analyzing scanned blots using ImageJ software. Phosphorylated protein levels were normalized to total protein. Data are representative of three independent experiments (one-way ANOVA, p-values have been provided). Sham, n=5; MI-vehicle, n=5, MI-PF, n=8.

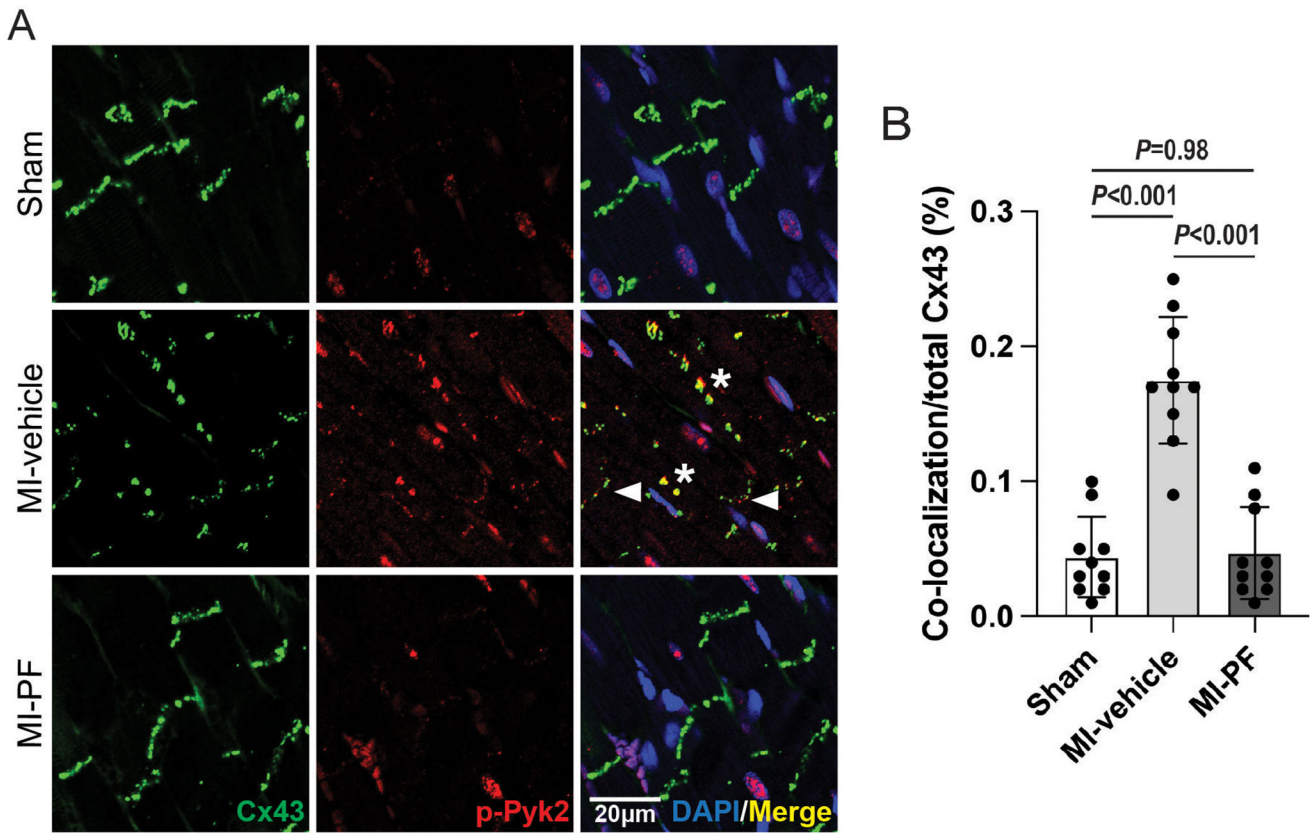

Figure 5. Effect of PF4618433 on the cellular localization of active Pyk2 and Connexin43 in the myocardial infarction rat heart.

A) Left ventricle tissue (distal to the infarction, hypertrophy area) from 6-weeks after Sham or left anterior descending artery ligation treated without (Myocardial infarction (MI)-vehicle) or with PF4618433 (MI-PF) were harvested for immunofluorescence imaging (green, Connexin (Cx43); red, enhanced active Pyk2, p-Pyk2Y579/580; yellow, co-localization; blue, DAPI; white arrows, intercalated disc; stars, lateral membrane). B) Quantification of Cx43 and Pyk2 co-localization (one-way ANOVA, p-values have been provided). Sham, n=10; MI-vehicle, n=10, MI-PF, n=10. Scale bar = 20 μm.

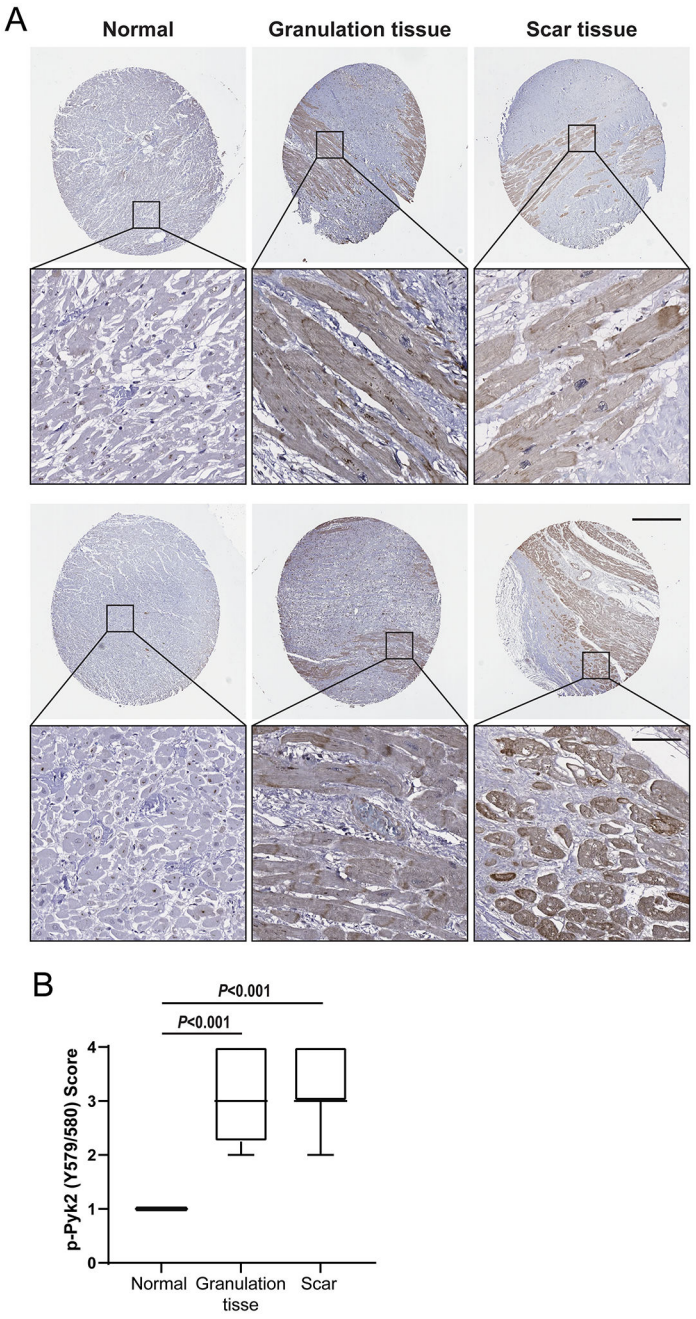

Figure 6. Level of active Pyk2 in human myocardial infarction samples.

A) Representative immunohistochemical images of active Pyk2 (pY579/580) in tissue microarray sections from normal and diseased (Granulation and Scar tissue) samples. Tissue spot diameter is 2 mm and the field of view for each sample was 40x. B) Boxplots depicting distribution of active Pyk2 (pY579/580) staining scores when combining each sample in normal (n=4), Granulation tissue (n=8), and Scar tissue (n=12) groups (one-way ANOVA, p-values have been provided). Scale bar (top) = 400 μm, Scale bar (bottom) = 50 μm.

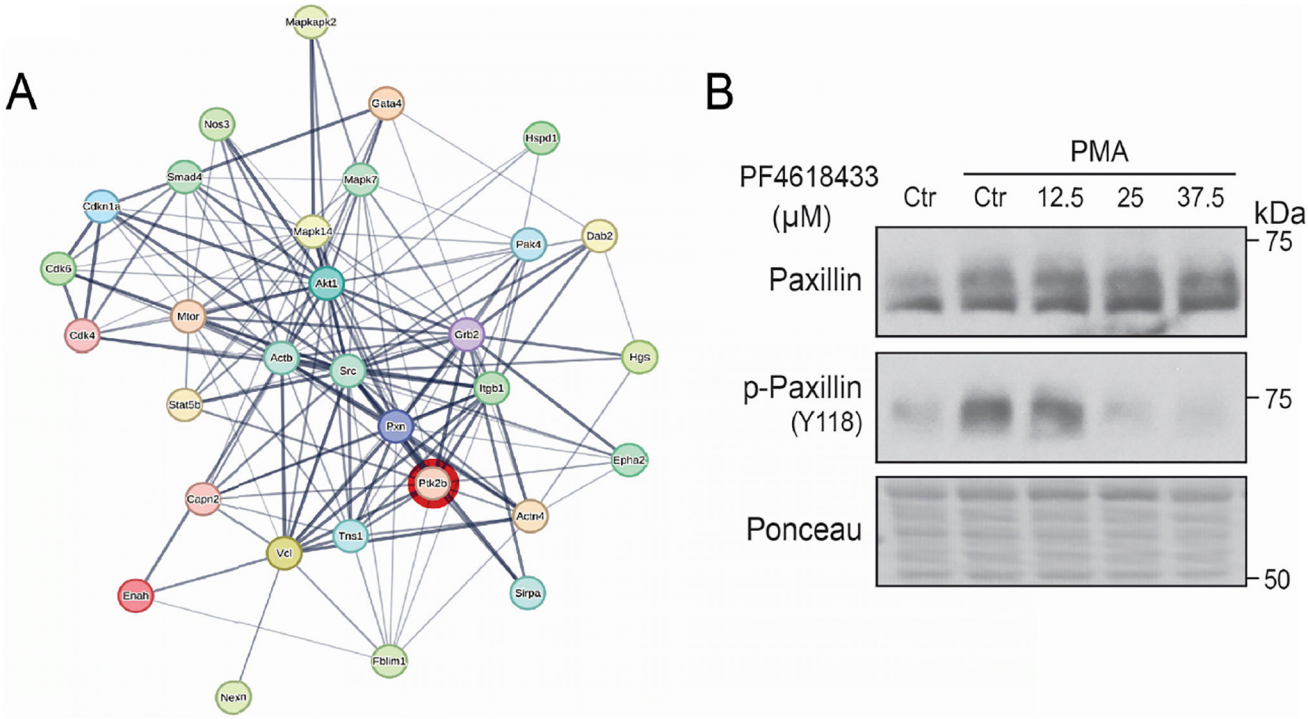

Figure 7. HUB gene network construction of Pyk2 specific proteins in STRINGdb.

A) In the PPI network construction, common 30 hub genes with close correlation were identified which are highly enriched in all the modules. Thickness of the edges indicate confidence level between two proteins which have shared functions. Red circle, Ptk2b (Pyk2 gene). B) Lysate from HeLa^{Cx43} cells treated with PF4618433 and Phorbol 12-myristate 13-acetate (PMA, 100 nM, 1 hr) were Western blotted. Antibodies used are labeled on the left of each panel.

Table I.

Comparison of heart rate and conventional echocardiographic parameters 6-weeks post myocardial infarction (MI), with and without PF4618433 (PF) treatment.

Groups	Sham	MI-vehicle	MI-PF	p-value
Cardiac output (ml/min)	64.4±2.7	42.0±5.7	67.8±5.6	0.009
LV end-diastolic Diameter (mm)	7.7±0.2	10.6±0.3	10.7±0.3	<0.001
LV end-systolic Diameter (mm)	4.5±0.2	9.3±0.3	9.0±0.2	<0.001
Ejection Fraction (%)	71.4±1.4	24.1±1.7	31.8±1.5	<0.001
Fractional Shortening (%)	42.2±1.2	11.8±0.9	16.0±0.9	<0.001
LV Mass (mg)	960.2±46.5	1315.8±66.6	1452.9±59.8	<0.001
LV Mass Corrected (mg)	768.1±37.2	1052.7±53.3	1162.4±47.8	<0.001
Stroke Volume (μL)	228.0±9.3	153.6±12.0	206.4±14.8	0.006
LV end-diastolic Volume (μL)	320.6±16.5	637.9±40.0	661.1±35.0	<0.001
LV end-systolic Volume (μL)	92.6±8.3	484.3±33.4	450.5±25.2	<0.001